# Orientational Order and Dynamics of Hydration Water in a Single Crystal of Bovine Pancreatic Trypsin Inhibitor

Kandadai Venu,* L. Anders Svensson,# and Bertil Halle*
*Condensed Matter Magnetic Resonance Group and #Molecular Biophysics, Department of Chemistry, Lund University, Lund, Sweden

ABSTRACT The orientational order and dynamics of the water molecules in form II crystals of bovine pancreatic trypsin inhibitor (BPTI) are studied by $^2$H NMR in the temperature range 6–50°C. From the orientation dependence of the single crystal quadrupole splitting and linewidth, the principal components of the motionally averaged quadrupole interaction tensor and the irreducible linewidth components for the orthorhombic crystal are determined. With the aid of water orientations derived from neutron and x-ray diffraction, it is shown that the NMR data can be accounted for by a small number of highly ordered crystal waters, some of which have residence times in the microsecond range. Most of these specific hydration sites must be located at intermolecular contacts. The surface hydration layer that is also present in dilute solution is likely to be only weakly ordered and would then not contribute significantly to the splitting and linewidth from the protein crystal. To probe water dynamics on shorter time scales, the $^2$H longitudinal relaxation dispersion is measured for a polycrystalline BPTI sample. The observed dispersion is dominated by rapidly exchanging deuterons in protein side chains, undergoing restricted rotational motions on a time scale of 10 ns.

## INTRODUCTION

Our understanding of protein structure and dynamics is largely derived from two experimental techniques: x-ray/neutron diffraction and nuclear magnetic resonance. Any attempt to compare results from these techniques faces the problem that diffraction data pertain to protein molecules densely packed into a crystal lattice, whereas NMR data usually refer to effectively isolated protein molecules in a dilute (mM) aqueous solution. Because the water content of the crystal is often below what is required for uniform monolayer coverage, at least for small proteins (Matthews, 1968; Islam and Weaver, 1990), crystal packing interactions may substantially alter the structure, dynamics, and solvation of the protein surface. Water-mediated protein interactions are also crucial for crystal stability (Frey, 1994; Nagendra et al., 1998).

Diffraction data have provided a wealth of information about the spatial distribution of water molecules in and around proteins in the crystal lattice (Baker, 1995), and two complementary NMR techniques, magnetic relaxation dispersion (MRD) (Halle et al., 1999) and nuclear Overhauser effect (NOE) spectroscopy (Otting, 1997), have been used to characterize the dynamics of hydration water for proteins in solution. To date, both diffraction and NMR techniques have provided more detailed and reliable information about internal (buried) water molecules than about the surface hydration of proteins. The thermal *B* factors obtained from diffraction data reflect positional order, but little is known about the orientational order of water molecules at protein surfaces. Orientational order parameters have been determined for internal water molecules by relaxation dispersion measurements (Denisov et al., 1997) and for surface water in clays and amphiphilic liquid crystals by solid-state NMR (Halle and Wennerström, 1981). Another unresolved aspect of protein hydration concerns the residence times of water molecules at hydration sites on the surface. Both MRD and NOE studies indicate subnanosecond residence times at exposed surface sites (Denisov and Halle, 1996; Iwai et al., 1998), but the small crystallographic *B* factors for many such sites suggest highly localized water molecules (Baker, 1995). These findings are not necessarily incompatible (Edsall and McKenzie, 1983), inasmuch as the dynamic and structural aspects reflect complementary regions of configurational space: *B* factors sample the most probable configurations, whereas residence times are governed by improbable configurations (barriers or saddle points on the potential-of-mean-force hypersurface). Yet it is not inconceivable that surface waters are more long-lived in the crystal than in solution. In particular, water molecules residing in cavities or deep pockets created by crystal contacts may have residence times comparable to those of internal water molecules.

In the present study, we use solid-state NMR to assess the orientational order and dynamics of surface hydration in a protein crystal. Specifically, we record the orientation dependence of the quadrupole splitting and linewidth in the water $^2$H spectrum from a single crystal of bovine pancreatic trypsin inhibitor (BPTI) in the temperature range 6–50°C. The first water NMR studies of protein crystals used the $^1$H isotope (Krüger and Helcké, 1967; Hsi et al., 1976; Bryant et al., 1982). Because of complications with intermolecular cross-relaxation (Hsi and Bryant, 1977) and

*Received for publication 23 November 1998 and in final form 12 April 1999.*

Address reprint requests to Dr. Bertil Halle, Condensed Matter Magnetic Resonance Group, Chemical Center, Lund University, P.O. Box 124, S-22100 Lund, Sweden. Tel.: 46-46-222-9516; Fax: 46-46-222-4543; E-mail: bertil.halle@fkem2.lth.se.

Dr. Venu's present address is School of Physics, University of Hyderabad, Hyderabad 500046, India.



0006-3495/99/08/1074/12 $2.00

proton-exchange averaging of the dipolar splitting (Lauterbur et al., 1978), the $^2$H isotope has been favored in later work (Lauterbur et al., 1978; Borah and Bryant, 1982; Usha and Wittebort, 1989; Usha et al., 1991). The present study goes further in several respects. We have determined the principal components of the motionally averaged quadrupole interaction tensor from the orientation dependence of the $^2$H quadrupole splitting from a single crystal, with the crystal axes identified by x-ray diffraction. We have also determined the irreducible linewidth components of the orthorhombic crystal from the orientation dependence of the linewidth. These model-independent results were analyzed with the aid of the jointly refined x-ray/neutron structure of BPTI, which provides orientations for 63 of the 160 crystal waters. The analysis indicates that the quadrupole splitting is due to a small number of highly ordered crystal waters, most of which are probably located at intermolecular contacts. A subset of these ordered water molecules may have residence times in the microsecond range and can then account for the large orientation-dependent $^2$H linewidth. Most water molecules in contact with the protein surface are probably weakly ordered, but their contributions to the quadrupole splitting tend to cancel out because of fast exchange within a nearly isotropic distribution of hydration sites. Finally, we measured the $^2$H relaxation dispersion in the range 2–55 MHz from polycrystalline BPTI. We conclude that the longitudinal relaxation rate is dominated by labile BPTI deuterons and that the rotational motion of the majority of crystal waters is slower than in bulk water by less than an order of magnitude. The physical properties of water in protein crystals as studied here are of interest not only as they relate to protein hydration under physiological solution conditions, but also in connection with crystal enzymology (Makinen and Fink, 1977; Mozzarelli and Rossi, 1996) and relaxation-based contrast in magnetic resonance imaging.

## MATERIALS AND METHODS

### Protein crystals

BPTI, generously supplied by Novo Nordisk A/S (Gentofte, Denmark), was dialyzed (3.5-kDa cutoff) against deionized, double-distilled water and then lyophilized. Form II crystals of BPTI were grown in $D_2O$ (>99.8 atom% D), essentially as described previously (Walter and Huber, 1983; Wlodawer et al., 1984). A 100 mg ml$^{-1}$ solution of purified BPTI in $D_2O$ was mixed with 0.5 M potassium phosphate buffer (in $D_2O$) of pH* 9.5 (uncorrected meter reading) in a volume ratio of 5:2. This solution was left in a sealed container together with a buffer reservoir (5–10 times the volume of the crystallization solution). After 2–3 weeks, many small crystals of tetragonal bipyramidal shape were observed in the crystallization solution. These crystals were used for polycrystalline NMR samples.

Large single crystals for orientation-dependent NMR experiments were grown by the macroseeding technique. A crystallization solution prepared as described above was filtered (0.22 $\mu$m) to minimize heterogeneous nucleation by dust particles (Blow et al., 1994) and allowed to equilibrate for 4 days in a sealed container in the presence of excess buffer. The crystallization solution was then seeded with crystals that were washed in buffer after being taken from the first batch. After ~6 weeks, these crystals had grown to suitable size, typically $4 \times 3 \times 1$ mm$^3$.

Several crystals prepared in this way were examined by x-ray diffraction on a Rigaku RU200BEH rotating Cu anode diffractometer operating at 45 kV and 90 mA with a focus of $0.3 \times 0.3$ mm. Diffraction patterns were collected with a Siemens X1000 area detector system and evaluated with the programs XDS and SADIE (Siemens software). The crystals were found to belong to the orthorhombic space group $P2_12_12_1$, with lattice constants $a = 74.2$ Å, $b = 23.4$ Å, and $c = 28.9$ Å, as expected for crystal form II (Walter and Huber, 1983; Wlodawer et al., 1984). This x-ray analysis also established the orientation of the principal axes: the *c*-axis is along the longest dimension, and the *b*-axis is along the shortest dimension of the crystal.

### NMR measurements

Deuteron ($^2$H) NMR spectra from a single crystal of BPTI were recorded as a function of the orientation of the crystal with respect to the magnetic field. The crystal was allowed to dry on a filter paper for a few minutes and was then mounted (with the aid of Parafilm) in a close-fitting cylindrical bore drilled through the center of a Teflon cube, with the crystallographic axes approximately aligned with the cube axes. The Teflon cube was then inserted in a tight-fitting NMR tube with an attached goniometer arrangement (2° accuracy). By rotating the NMR tube around its axis (perpendicular to the magnetic field), the crystal could thus be rotated around any of the three crystal axes, depending on how the cube was inserted in the tube.

To prevent the single crystal from drying and fracturing (Borah and Bryant, 1982) during the course of the experiment, a filter paper saturated with mother liquor was placed inside the NMR tube, well removed from the RF coil. Crystals mounted in this way remained stable and gave reproducible spectra over a period of several weeks. The spectra were also reproducible after extensive sample rotation, change of rotation axis, and temperature variation, showing that the crystal did not move during these manipulations and did not dehydrate, even at 50°C.

NMR spectra were recorded on a Bruker DMX-200 spectrometer equipped with high-power accessories for experiments on solids. The 90° pulse length was ~5 $\mu$s. Both a quadrupolar echo sequence, with a pulse delay of 25 $\mu$s, and single pulse excitation with similar acquisition delay were used. Typically, 4000 transients were averaged. Quadrupolar echo and single pulse spectra did not differ significantly, and both were independent of delay time (25–200 $\mu$s), showing that slow-motion effects on the lineshape are unimportant (Spiess and Sillescu, 1981; Wittebort et al., 1987). The reported single crystal data were obtained from single pulse spectra. Powder spectra covering the broad spectral component due to slowly exchanging deuterons were recorded on the same spectrometer, using a 5-mm probe with a 3-$\mu$s 90° pulse. Orientation-dependent single crystal lineshapes were recorded at three temperatures, 6°C, 27°C, and 50°C, using a gas flow temperature controller with 0.5°C accuracy and 0.1°C stability.

$^2$H longitudinal relaxation time measurements on polycrystalline samples were carried out in the frequency range 2–55 MHz, using Nicolet 360, Bruker DMX-200, DMX-100, and MSL spectrometers. The pulse sequence consisted of a 180° inversion pulse, followed, after a variable evolution time, by a quadrupolar echo detection sequence. All inversion recovery curves were single-exponential within the experimental accuracy.

## RESULTS

### Polycrystalline samples

Fig. 1 shows the $^2$H NMR spectrum from a polycrystalline sample of crystal form II of BPTI. As previously observed for other proteins (Usha and Wittebort, 1989; Usha et al., 1991), the spectrum consists of a broad, weakly biaxial powder lineshape superimposed on a narrow component with an unresolved powder lineshape. The broad component is due to slowly exchanging deuterons in peptide groups and

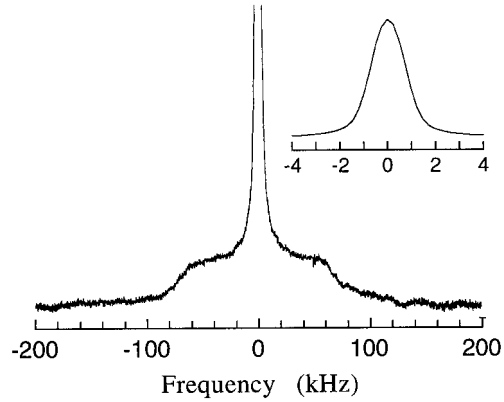


FIGURE 1 $^2$H NMR spectrum from a polycrystalline sample of form II crystals of BPTI at pH* 9.5 and 27°C. The inset shows the narrow central line on an expanded frequency scale.

side chains of the protein and in a few trapped water molecules (see below), and the narrow component is due to the majority of the crystal waters, exchanging on a submicrosecond time scale (Usha and Wittebort, 1989; Usha et al., 1991). Quantitative intensity measurements were not attempted, but a crude estimate is consistent with the expected 25% of slowly exchanging deuterons (see below). Because we are primarily interested in the crystal water, we focus on the narrow component. To observe the splitting of this component, however, it is necessary to use a single crystal.

## Orientation-dependent quadrupole splitting

Fig. 2 shows typical $^2$H NMR spectra from a form II single crystal of BPTI. As expected for a spin-1 nucleus in an anisotropic system (Abragam, 1961), the spectrum is a symmetrical doublet of Lorentzian lines. This quadrupole doublet is due to water molecules exchanging among the different hydration sites in the crystal on a submicrosecond time scale (see Discussion).

The spectra in Fig. 1 also contain a sharp central line, as previously observed in $^2$H spectra from a single crystal of lysozyme and then attributed to water in the interstitial spaces of the crystal, sufficiently removed from the ordering influence of the protein surface (Borah and Bryant, 1982). This explanation, however, requires the exchange between interstitial water and ordered water (responsible for the doublet) to be slower than milliseconds (the inverse of the splitting), otherwise the isotropic fraction would simply reduce the magnitude of the splitting. Such slow exchange is not consistent with the current understanding of protein hydration dynamics (Halle, 1999). Instead, we attribute the central line to water adsorbed on macroscopic surfaces, i.e., on the inside of the NMR tube, on the surfaces of the Teflon cube, on the Parafilm used to mount the crystal, and on the crystal itself. This explanation is consistent with the absence of an isotropic peak in $^2$H spectra from polycrystalline protein samples and with the finding that the isotropic peak disappears below the freezing point of bulk water (Borah and Bryant, 1982), whereas the motionally averaged powder lineshape from crystal water disappears gradually and reaches the rigid-lattice limit only below 200 K (Usha and Wittebort, 1989; Usha et al., 1991). When examined in detail, the central line was found to have a weakly orientation-dependent fine structure, presumably reflecting magnetic field inhomogeneity and susceptibility effects.

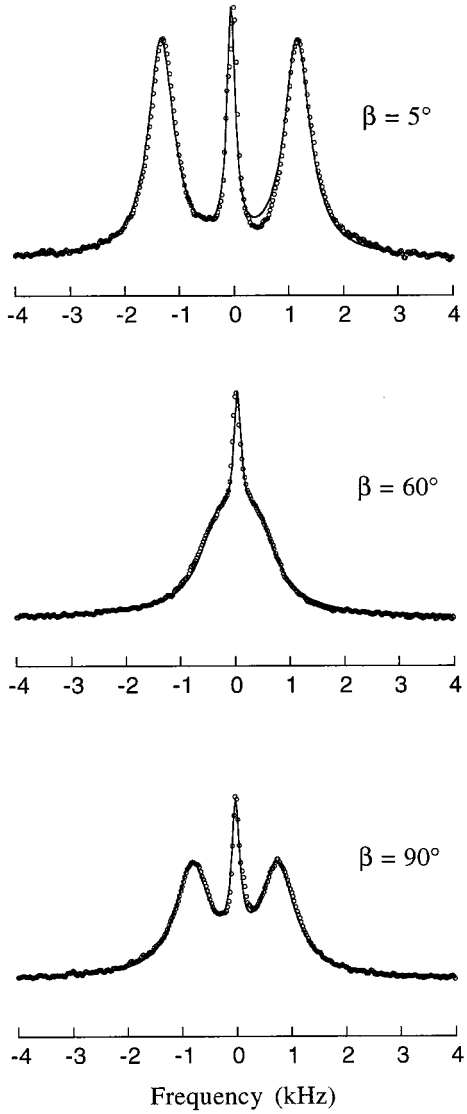


FIGURE 2 $^2$H NMR spectra from a form II single crystal of BPTI at pH* 9.5 and 27°C. The rotation angle, $\beta$, around crystal axis $c$ (configuration I) is indicated. The curves were obtained from fits to a symmetrical doublet plus a Lorentzian central line.

The quadrupole doublet is fully characterized by two parameters: the quadrupole splitting, $\nu_Q$, and the homogeneous linewidth, $\Delta\nu$. When the splitting is large compared to the linewidth, these parameters can be obtained directly as the frequency separation of the two peaks and the half-amplitude width of either peak, respectively. When the doublet peaks overlap (as in the 60° and 90° orientations of Fig. 2), accurate estimation of $\nu_Q$ and $\Delta\nu$ requires a lineshape analysis. All reported $\nu_Q$ and $\Delta\nu$ values were obtained

by fitting a superposition of a symmetrical doublet (two parameters) and a Lorentzian line (three parameters: width, offset, and relative weight) to the experimental spectra. The fact that the central line is not strictly Lorentzian had no significant effect on the relevant parameters $\nu_Q$ and $\Delta\nu$. The curves in Fig. 2 resulted from such fits.

The single crystal quadrupole splitting $\nu_Q$ is proportional to the component of the quadrupole interaction tensor along the static magnetic field and therefore depends on the orientation of the crystal with respect to the field as seen in Fig. 3. By measuring the splitting as a function of crystal orientation, the principal components of the motionally averaged quadrupole tensor can be determined. For an orthorhombic crystal like the present one, the principal axis system of this tensor must coincide with the crystallographic axes. The principal components are therefore denoted $\nu_{aa}$, $\nu_{bb}$, and $\nu_{cc}$. Because the quadrupole tensor is traceless, only two components are independent. These components were determined by recording $\nu_Q$ as a function of the rotation angle $\beta$ in two configurations: (I) rotation around the *c*-axis with the *b*-axis parallel to the magnetic field at $\beta = 0$, and (II) rotation around the *b*-axis with the *c*-axis parallel to the magnetic field at $\beta = 0$. For these configurations,

$$\nu_Q^{I}(\beta) = \sin^2\beta\ \nu_{aa} + \cos^2\beta\ \nu_{bb} \quad (1a)$$

$$\nu_Q^{II}(\beta) = \sin^2\beta\ \nu_{aa} + \cos^2\beta\ \nu_{cc} = -\cos(2\beta)\ \nu_{aa} - \cos^2\beta\ \nu_{bb} \quad (1b)$$

In practice, it is not possible to perfectly align the crystal with the goniometer cube (see Materials and Methods). We therefore performed the transformation from the laboratory frame (defined by the magnetic field) to the crystal frame in two steps, via the cube frame. This introduces a set of three Euler angles, $(\alpha', \beta', \gamma')$, which bring the crystal frame into coincidence with the cube frame (Brink and Satchler, 1968). When $\beta'$ is small, the angular coefficients essentially depend on $\alpha' + \gamma'$, so we can set $\gamma' = 0$. The four independent parameters $\nu_{aa}$, $\nu_{bb}$, $\alpha'$, and $\beta'$ were determined by simultaneous fits to the experimental $\nu_Q(\beta)$ data for the two configurations I and II. The resulting fits are shown in Fig. 3, and the parameter values are collected in Table 1. It is seen that the misorientation angles $\alpha'$ and $\beta'$ are indeed small.

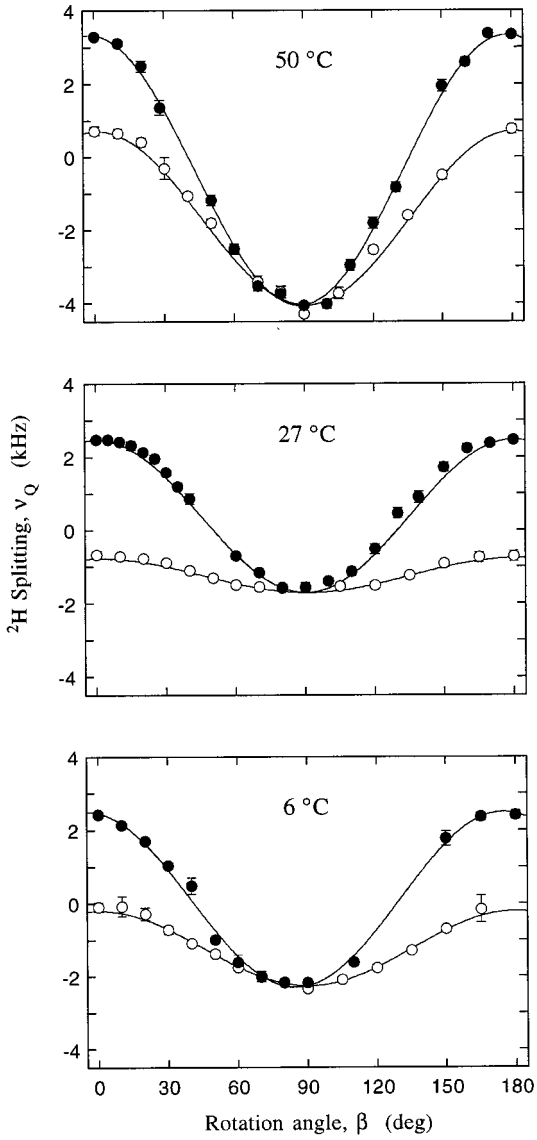


FIGURE 3 $^2$H quadrupole splitting from a form II single crystal of BPTI at pH* 9.5 and the indicated temperature. The angle, $\beta$, refers to rotation around crystal axis *c* (configuration I, ●) or to rotation around crystal axis *b* (configuration II, ○). The curves resulted from fits to all data at a given temperature; the resulting parameter values are given in Table 1.

## Orientation-dependent linewidth

As shown in Fig. 4, the linewidth $\Delta\nu$ depends on the orientation of the crystal with respect to the magnetic field. As for the quadrupole splitting, the mathematical form of this orientation dependence follows directly from the rotational symmetry of the crystal (Gustafsson and Halle, 1993). The orientation dependence can therefore be analyzed in a model-independent way, without invoking a dynamic model for the transverse relaxation that determines the homogeneous linewidth. (The invariance of the lineshape with re-

**TABLE 1 Parameter values derived from fits to orientation-dependent $^2$H lineshapes from a form II single crystal of BPTI at pH* 9.5**

| | 6°C | 27°C | 50°C |
|---|---|---|---|
| $\nu_{aa}$ (kHz)* | −2.29 ± 0.02 | −1.71 ± 0.03 | −4.05 ± 0.04 |
| $\nu_{bb}$ (kHz)* | 2.50 ± 0.03 | 2.48 ± 0.03 | 3.34 ± 0.03 |
| $\alpha'$ (deg.) | 5.0 ± 0.4 | −0.1 ± 0.5 | 1.9 ± 0.4 |
| $\beta'$ (deg.) | −0.3 ± 0.6 | −4 ± 8 | −0.9 ± 0.5 |
| $\Delta\nu_{A_{1(00)}}$ (Hz) | 268 ± 10 | 328 ± 10 | 389 ± 10 |
| $\Delta\nu_{A_{1(20)}}$ (Hz) | 20 ± 8 | −68 ± 6 | −131 ± 15 |
| $\Delta\nu_{A_{1(22)}}$ (Hz) | 310 ± 9 | 344 ± 8 | 533 ± 10 |
| $\Delta\nu_{B_1}$ (Hz) | 446 ± 28 | 531 ± 16 | 865 ± 44 |
| $3\Delta\nu_{B_2} - \Delta\nu_{B_3}$ (Hz) | 506 ± 20 | 620 ± 20 | 766 ± 20 |

*Only the relative signs of $\nu_{aa}$ and $\nu_{bb}$ can be determined from the data.

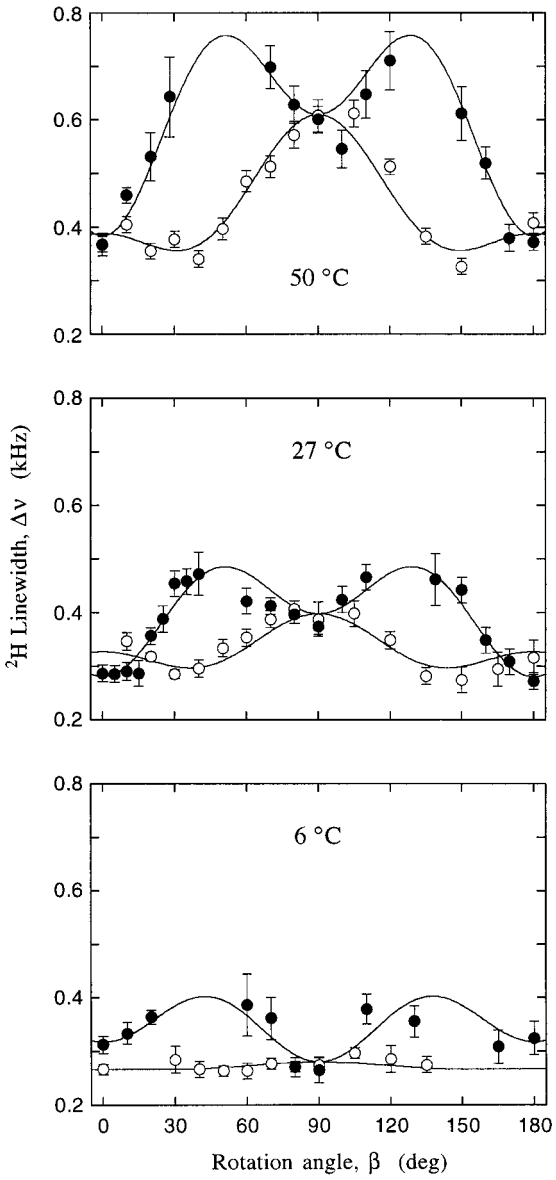


FIGURE 4 $^2$H linewidth from a form II single crystal of BPTI at pH* 9.5 and the indicated temperature. The angle, $\beta$, refers to rotation around crystal axis $c$ (configuration I, ●) or to rotation around crystal axis $b$ (configuration II, ○). The curves resulted from fits to all data at a given temperature; the resulting parameter values are given in Table 1.

spect to variation of the pulse delay in the quadrupolar echo sequence shows that slow-motion effects are unimportant.)

For an orthorhombic crystal (point group $\mathcal{D}_{2h}$), the linewidth can be expressed as a linear combination of six irreducible linewidth components according to (Gustafsson and Halle, 1993)

$$\Delta\nu = \sum_{\lambda} F_{\lambda}(\theta, \phi)\Delta\nu_{\lambda} \qquad (2)$$

where $\theta$ and $\phi$ are the spherical polar angles that specify the orientation of the magnetic field with respect to the crystal axes and the $\lambda$ sum runs over the six irreducible representations of the point group $\mathcal{D}_{2h}$. The angular functions $F_{\lambda}$ are given explicitly in Table 2 as functions of the rotation angle $\beta$ for configurations I and II. Because the irreducible representations $B_2$ and $B_3$ have the same angular coefficients (to within a numerical constant) for these configurations, only a linear combination of the corresponding linewidth components could be determined. We thus determined five independent linewidth components from simultaneous fits to the experimental $\Delta\nu(\beta)$ data for the two configurations. The resulting fits are shown in Fig. 4, and the parameter values are given in Table 1. Because the misorientation angles $\alpha'$ and $\beta'$ were found to be small, perfect alignment of crystal and cube was assumed in these fits.

## Magnetic relaxation dispersion

Fig. 5 shows the frequency dependence in the range 2–55 MHz of the longitudinal relaxation rate, $R_1$, of the narrow component (see Fig. 1) of the $^2$H spectrum from a polycrystalline sample of form II BPTI crystals. The nearly fivefold variation of $R_1$, implies that the longitudinal relaxation in this frequency range is dominated by motions with correlation times of order 10 ns. Because a low-frequency plateau is not evident, it would not be meaningful to fit a Lorentzian dispersion function to the data. Indeed, a previously reported water $^1$H dispersion from monoclinic lysozyme crystals shows no tendency to level out, even at 10 kHz (Bryant et al., 1982). On the other hand, the $R_1$, dispersion observed here is not just the high-frequency tail of a Lorentzian dispersion centered at lower frequency, because the observed frequency dependence is much weaker than inverse-square (cf. *dashed curve* in Fig. 5).

## DISCUSSION

A major issue in water $^2$H NMR studies of protein crystals is the origin of the observed quadrupole splitting and relaxation behavior ($R_1$ and linewidth). As seen by a water molecule, a protein crystal is a highly heterogeneous system comprising nearly isotropic interstitial regions, highly ordered buried hydration sites, and everything between these extremes. Although nearly all crystal waters contribute to the spectral intensity of the quadrupole doublet, it remains to establish the contributions of the different types of crystal water to the splitting and the linewidth.

**TABLE 2 Orientation-dependent coefficients of irreducible linewidth components for an orthorhombic crystal**

| | Configuration I | Configuration II |
|---|---|---|
| $A_1(00)$ | 1/4 | $(1/4)\ (3\cos^2\beta - 1)^2$ |
| $A_1(20)$ | $(\sqrt{3}/2)\cos(2\beta)$ | $(\sqrt{3}/2)\sin^2\beta\ (3\cos^2\beta - 1)$ |
| $A_1(22)$ | $(3/8)\ [1 + \cos(4\beta)]$ | $(3/4)\sin^4\beta$ |
| $B_1$ | $(3/8)\ [1 - \cos(4\beta)]$ | 0 |
| $B_2$ | 0 | $(9/2)\sin^2\beta\cos^2\beta$ |
| $B_3$ | 0 | $-(3/2)\sin^2\beta\cos^2\beta$ |

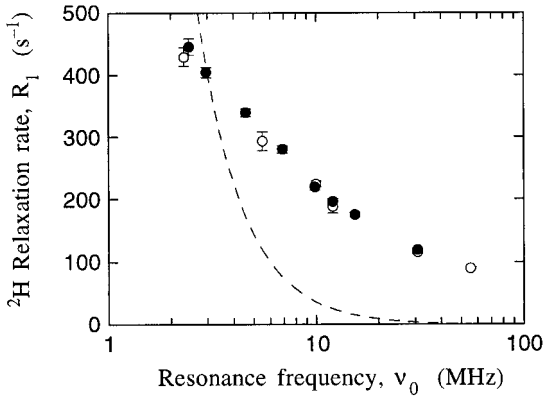


FIGURE 5 Frequency dependence of the $^2$H longitudinal relaxation rate, $R_1$, from a polycrystalline sample of form II crystals of BPTI at pH* 9.5 and 27°C. The symbols refer to two different crystal batches. The dashed curve illustrates an inverse-square frequency dependence.

## Water ordering in protein crystals

The $^2$H NMR spectrum from a polycrystalline protein sample at ambient temperature consists of a broad (~200 kHz) powder-like component and a narrow (~2 kHz) featureless component (Fig. 1). The narrow component appears as a resolved, orientation-dependent quadrupole doublet in single crystal spectra (Fig. 2). The broad component is due to deuterons that exchange slowly compared to their local quadrupole frequencies. Typically, this implies a residence time longer than ~1 $\mu$s. The narrow component, on the other hand, is due to rapidly exchanging deuterons, with residence times shorter than ~1 $\mu$s. It has been shown for crambin, lysozyme, and ribonuclease A (at 14°C) that the integrated intensities of the broad and narrow spectral components are in approximately the same ratio as the fractions of labile protein deuterons and crystal water deuterons, respectively (Usha and Wittebort, 1989; Usha et al., 1991). Within our modest accuracy, this is also the case for BPTI.

The exchangeable deuterons in crystal form II of BPTI at pH* 9.5 comprise 320 water deuterons (see below) and 104 labile BPTI deuterons (backbone peptide and side-chain amide, ammonium, guanidinium, and hydroxyl). If all labile deuterons exchange slowly and all water deuterons exchange rapidly, the relative intensity of the broad component would thus be 24.5%. For BPTI *in solution*, the hydrogen exchange rate constants are known for most of the labile hydrogens (Wagner, 1983; Tüchsen and Woodward, 1985; Liepinsh et al., 1992; Denisov and Halle, 1995). Using these rate constants, we find that all labile deuterons in BPTI at pH* 9.5 and 27°C have residence times much longer than 1 $\mu$s. In the crystal, exchange should be even slower. This has been demonstrated for the most slowly exchanging peptide hydrogens in BPTI (Gallagher et al., 1992) and lysozyme (Pedersen et al., 1991). Furthermore, labile deuterons in exposed side chains should exchange more slowly in the crystal because of the reduced accessibility of side chains near crystal contacts and the hindered diffusion of hydroxyl ions through the crystal lattice. (At pH* 9.5, there is one hydroxyl ion per $10^4$ BPTI molecules.) It seems safe to assume, therefore, that labile BPTI deuterons do not contribute to the single crystal quadrupole doublet, even at 50°C.

Although all previous water $^2$H NMR studies of protein crystals have reported water quadrupole splittings of the same order of magnitude (1–2 kHz) as found here for BPTI, a consensus interpretation has not emerged. Lauterbur et al. (1978) reported the orientation dependence of the splitting (max. 1.25 kHz) with rotation around three mutually perpendicular axes of an orthorhombic single crystal of lysozyme (40 vol% solvent). Because the relation of the rotation axes to the crystal axes was not established, however, the rotation patterns could not be quantitatively analyzed. Borah and Bryant (1982) measured a splitting (max. 1.9 kHz) from a monoclinic single crystal of lysozyme (33 vol% solvent), but found no splitting in an amorphous lysozyme powder of similar water content. These observations prompted the authors to rule out specific intramolecular hydration sites (assumed to remain intact in the powder sample) as the origin of the splitting. This argument does not appear convincing to us, however, because water molecules exchanging rapidly with such sites are expected to produce a splitting in a crystal, where the protein molecules have the same orientation in all unit cells, but not in an amorphous powder, where the protein molecules are isotropically distributed. Usha and Wittebort (1989) studied powder lineshapes from polycrystalline samples of monoclinic crambin (33 vol% solvent), and these studies were extended by Usha et al. (1991) to polycrystalline samples of monoclinic (33 vol% solvent) and tetragonal (42 vol% solvent) lysozyme and monoclinic ribonuclease A (46 vol% solvent). These studies focused on the broad component of the powder spectrum, dominated by slowly exchanging peptide deuterons, but an unresolved powder splitting of less than 2 kHz (at 287 K) was also inferred and attributed to orientationally disordered crystal water.

Form II crystals of BPTI contain 38 vol% solvent (Wlodawer et al., 1984). From the unit cell dimensions (see Materials and Methods) and the bulk water molar volume of 30.0 Å$^3$ (assumed to apply also to crystal water), it then follows that the crystal contains 160 water molecules per protein. (The small corrections for the four internal water molecules and a phosphate and a potassium ion from the mother liquor tend to cancel out.) The free BPTI molecule has a solvent-accessible surface area of 3900 Å$^2$. If each water molecule occupies 15 Å$^2$, this corresponds to a monolayer of 260 water molecules. In the crystal, 42.5% of the surface area is buried at protein contacts (Islam and Weaver, 1990), leaving 150 waters in contact with the exposed surface. In the joint refinement of 1.0-Å-resolution x-ray and 1.8-Å-resolution neutron diffraction data, 63 hydration sites were modeled with occupancies in the range 0.4–1.0 and thermal $B$ factors in the range 11–92 Å$^2$ (Wlodawer et al., 1984). Among these 63 hydration sites are four internal waters (W111–113 and W122) and about a dozen intermolecularly trapped waters residing in deep crevices and pock-

ets formed by contacts with one or two of the 14 nearest-neighbor protein molecules in the crystal. The crystallographically identified hydration sites also include many waters interacting with the exposed protein surface. About 100 waters, many of which make direct contact with the protein surface, are apparently not sufficiently positionally ordered to be crystallographically observable, even at very high resolution.

Although it seems clear that the quadrupole doublet is entirely due to crystal water, it is not obvious that all 160 waters are in the fast exchange limit. The residence time of the singly buried water molecule, W122, has been determined in solution as a function of temperature (Denisov et al., 1996): it ranges from 2.6 ms at 6°C to 13 $\mu$s at 50°C. Suppression of conformational fluctuations by crystal forces, as inferred from peptide hydrogen exchange experiments (Gallagher et al., 1992), should make the residence time of W122 even longer in the crystal. Whereas W122 therefore should not contribute to the quadrupole doublet, the situation is less clear for the remaining three internal water molecules, W111–113. These have residence times somewhere in the range 0.02–1 $\mu$s in solution at 27°C (Denisov et al., 1995) and may therefore go from slow to fast exchange with increasing temperature in the crystal. Form II crystals of BPTI also contain about a dozen intermolecularly trapped waters residing in deep crevices and pockets formed by two or three contacting protein molecules. In solution, these regions of the protein surface would be exposed and would therefore not be occupied by long-lived water molecules. In the crystal, however, some of these water molecules might have residence times longer than 1 $\mu$s.

The quadrupole splitting contains information about the orientational order of the rapidly exchanging water molecules. The principal components of the motionally averaged quadrupole interaction tensor may be expressed as

$$\nu_{\alpha\alpha} = \tfrac{3}{2}\chi A^{C}_{\alpha\alpha}, \quad \alpha = a, b, \text{or } c \tag{3}$$

where $\chi$ is the rigid-lattice water $^2$H quadrupole coupling constant, taken to be 213 kHz, as in ice Ih (Edmonds and Mackay, 1975). The crystal-frame residual anisotropies $A^{C}_{\alpha\alpha}$ represent the extent of motional averaging of the local quadrupole interaction tensor (fixed in the water molecule) with respect to the indicated crystal axis. Explicit expressions for these quantities are given in Appendix A. This motional averaging occurs at two levels: 1) by restricted rotational motions in a given hydration site, and 2) by exchange (translational diffusion) between hydration sites with different orientations (and different degrees of local order).

Although it is clearly not possible to obtain a detailed picture of water ordering in the many individual hydration sites from the two experimental observables $\nu_{aa}$ and $\nu_{bb}$, their magnitudes and temperature dependence can be used to discriminate among certain models. We shall consider two simple models for the orientational order of the water molecules in a protein crystal. In the first model, which we refer to as the *hydration layer model*, the quadrupole doublet is due to a large number of weakly ordered water molecules, essentially all waters in contact with exposed protein surfaces. For simplicity, we assume that the local order is uncorrelated with the orientation of the hydration site and that there is at least threefold local symmetry. Then we can factorize the crystal-frame residual anisotropies as (cf. Eq. A7)

$$A^{C}_{\alpha\alpha} = S_{\alpha\alpha}\langle A^{D}_{0}\rangle, \quad \alpha = a, b, \text{or } c \tag{4}$$

where $A^{D}_{0}$ is the local residual anisotropy defined in Eq. A2, and the angular brackets signify averaging over all hydration sites. The geometric order parameters $S_{\alpha\alpha}$ reflect the orientational distribution of the hydration sites. If all hydration sites were to have the water $C_{2v}$ axis preferentially aligned with the *c*-axis of the crystal, then $S_{cc} = 1$ and $S_{aa} = S_{bb} = -1/2$, and if the hydration sites were isotropically distributed, then $S_{aa} = S_{bb} = S_{cc} = 0$. Although the BPTI molecule is certainly not a smooth sphere, Fig. 6 shows that the crystallographically identified waters are rather uniformly distributed in orientational space. We therefore expect that $S_{\alpha\alpha} \ll 1$. This was verified by explicit calculation of $S_{\alpha\alpha}$, using the atomic coordinates of the 62 potentially contributing crystal waters (W122 was excluded). As seen from Fig. 7, $|S_{\alpha\alpha}| < 0.1$ already after inclusion of the 20 most highly (positionally) ordered waters (with smallest *B* factor).

As a test of the hydration layer model, we calculated the average local residual anisotropy $\langle A^{D}_{0}\rangle$ from Eqs. 3 and 4, using the experimental quadrupole frequencies $\nu_{aa}$ and $\nu_{bb}$ (Table 1) and the geometric order parameters in Fig. 7. (The reported $\langle A^{D}_{0}\rangle$ values are averaged over the *N* partially ordered water molecules rather than all 159 rapidly exchanging crystal waters. Before substitution into Eq. 4, this

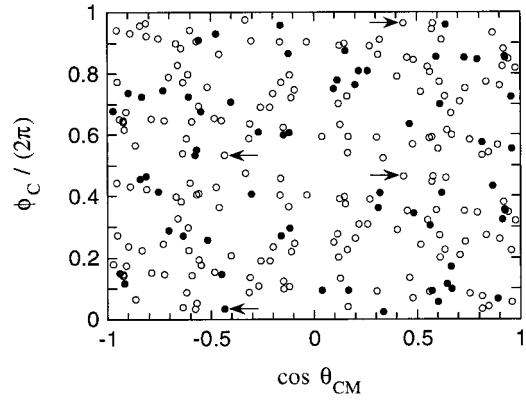


FIGURE 6 Orientational distribution for the 4 × 62 crystal waters (excluding W122) identified in the unit cell of crystal form II of BPTI. The 62 waters in the asymmetrical unit (●) are shown along with symmetry-related waters in the unit cell (○). Four symmetry-related waters are identified by arrows. The spherical polar angles $\theta_{CM}$ and $\phi_C$ specify the orientation of the water $C_{2v}$ axis with respect to the crystal axes. An isotropic orientational distribution corresponds to a uniform distribution of points in the plane of the figure.

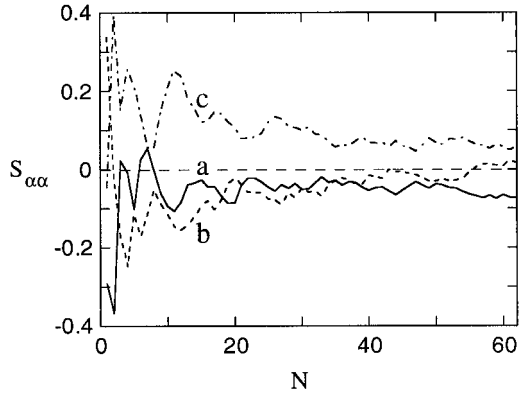


FIGURE 7 Geometric order parameters $S_{aa}$, $S_{bb}$, and $S_{cc}$, averaged over $N$ crystal waters (added in order of increasing $B$ factor). The orientations of the 62 waters (excluding W122) were calculated from the crystallographic coordinates.

value should be multiplied by a factor $N/159$, accounting for $159 - N$ waters with negligible residual anisotropy.) The results of this calculation, shown in Fig. 8, lead us to reject the hydration layer model because it requires an unreasonably high local order to account for the observed quadrupole splitting. The required magnitude of $\langle A_0^D \rangle$ is of order 1, nearly two orders of magnitude larger than for interfacial water in clays and amphiphilic liquid crystals (Halle and Wennerström, 1981). In fact, the $\langle A_0^D \rangle$ values in Fig. 8 mostly fall outside the theoretically allowed range, $-0.55 < A_0^D < 0.49$, which follows from Eqs. A2–A4 and the geometry of the water molecule. Moreover, the $\langle A_0^D \rangle$ values calculated from the two measured quadrupole frequencies $\nu_{aa}$ and $\nu_{bb}$ differ greatly (being mostly of opposite sign). Even if an unphysically large local order is admitted, the hydration layer therefore cannot simultaneously account for $\nu_{aa}$ and $\nu_{bb}$.

Having rejected a weakly ordered hydration layer as the origin of the quadrupole splitting, we now consider the possibility that a few highly ordered water molecules, exchanging rapidly (submicrosecond residence times) with the remaining (weakly ordered) waters, might account for the splitting data. To quantitatively assess this specific site model, we introduce the simplifying assumption that all water molecules that contribute to the splitting are fully ordered, and the remaining waters are isotropically disordered. The quadrupole frequencies $\nu_{aa}$ and $\nu_{bb}$ can then be calculated by means of Eqs. 3 and A6. The results of such calculations are shown in Fig. 9. Here, the first 16 waters include three internal waters (W111–113), 10 intermolecularly trapped waters (W110, 119, 129, 157, 200, 216, 218, 223, 302, and 304), and the three remaining waters with full occupancy and $B < 30$ Å$^2$ (W138, 143, and 203). These are the water molecules most likely to be highly (orientationally) ordered. It is seen that the quadrupole frequencies measured at the lower temperatures can be accounted for by as few as three ordered water molecules, whereas the 50°C data require about 10 ordered waters. The observed increase in the quadrupole frequencies with temperature can now be understood as the result of a small number of ordered waters going from a slow-exchange (residence time $> 1$ $\mu$s) to a fast-exchange ($<1$ $\mu$s) situation. In the calculation shown in Fig. 9, these water molecules are W111, 112, 113, 200, 203, and 302, whereas the 6°C splitting is due to W119, 143, and 223. Although plausible, this is by no means a unique assignment. By adding water molecules in different order, many different curves like the ones in Fig. 9 can be generated. Furthermore, whereas the quadrupole frequencies are accurate to ~1% (Table 1), there is a larger uncertainty associated with the water orientations deduced from the crystallographic coordinates (but the 16 selected waters are among the most accurately localized ones) (Wlodawer et al., 1984) and with the neglect of local disorder (Denisov et al., 1997). Nevertheless, this calculation demonstrates that the magnitude and temperature dependence of the quadrupole

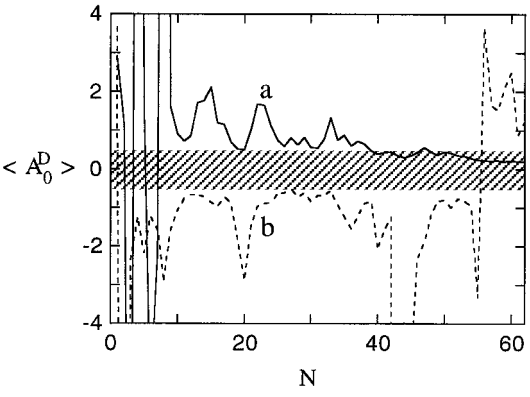


FIGURE 8 Local residual anisotropy, $A_0^D$, averaged over $N$ partially ordered crystal waters (added in order of increasing $B$ factor). $\langle A_0^D \rangle$ was calculated according to Eqs. 3 and 4, using the quadrupole tensor components $\nu_{aa}$ (*solid line*) and $\nu_{bb}$ (*dashed line*) measured at 50°C and the geometric order parameters $S_{aa}$ and $S_{bb}$ in Fig. 6. The theoretically allowed region for $\langle A_0^D \rangle$ is hatched.

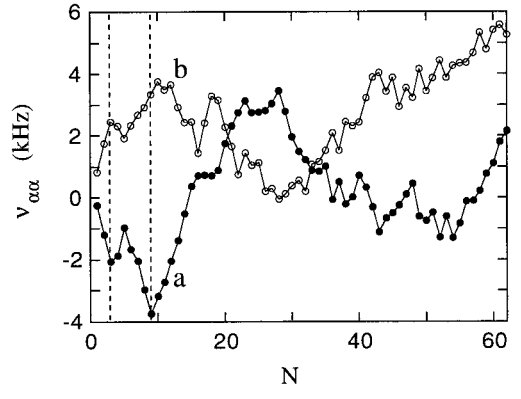


FIGURE 9 Quadrupole tensor components $\nu_{aa}$ (●) and $\nu_{bb}$ (○) calculated according to Eqs. 3 and A6 for $N$ fully ordered crystal waters and $159 - N$ isotropic waters. The first 16 waters include three internal (W111–113) and 10 intermolecularly trapped waters; the remaining 46 waters were added in order of increasing $B$ factor. The quadrupole frequencies measured at 6°C and 50°C (see Table 1) closely match the calculated frequencies for $N = 3$ and 9, respectively (*vertical dashed lines*).

frequencies can be explained by a small number of highly ordered water molecules. The minimum number of ordered water molecules required is three at 6°C and about nine at 50°C. These numbers would increase somewhat if we allowed for local disorder, but the presence of only ~15 buried and trapped waters (some of which may remain in the slow-exchange limit at 50°C) in the crystal structure suggests that the actual numbers are small.

## Water dynamics in protein crystals

Whereas quadrupole splittings are fully determined by equilibrium orientational distributions, spin relaxation rates and homogeneous linewidths also contain information about the rates of molecular motions. Because a protein crystal is heterogeneous with respect to orientational order as well as dynamics, it is not straightforward to extract the dynamic information. Furthermore, we must consider not only local water reorientation, but also translational diffusion (exchange) of ordered water molecules between sites differing in local order and/or orientation. Symmetrical 180° flips of ordered water molecules may also contribute (Fischer et al., 1998). Finally, contributions from labile BPTI deuterons cannot be ruled out.

We consider first the orientation-dependent linewidths (Fig. 4 and Table 1). Under the conditions of the present study, the irreducible linewidth coefficients can be expressed as (see Appendix B)

$$\Delta\nu_\lambda = \frac{1}{\pi N}\sum_k \frac{(\omega_{Qk}^\lambda)^2\tau_k}{1+(\omega_{Qk}^\lambda\tau_k)^2} \qquad (5)$$

where the sum runs over all ordered water molecules, with residence time $\tau_k$ and residual quadrupole frequency $\omega_{Qk}^\lambda = (3/2)\,\pi\chi G_\lambda(\Omega_{CM}^k)$, with $G_\lambda$ dependent on the orientation of the hydration site. Furthermore, $N = 160$ is the number of water molecules per BPTI molecule. The denominator in the summand of Eq. 5, which is an ad hoc extension of the rigorous result for the fast exchange limit, attenuates the contribution from slowly exchanging water molecules. Among the ordered waters, those with residence times near $1/\omega_{Qk}^\lambda \approx 1\ \mu s$ will therefore dominate the linewidth. Because Eq. 5 shows that a single ordered water molecule can contribute as much as 2000 $G_\lambda(\Omega_{CM}^k)$ Hz (where $G_\lambda(\Omega_{CM}^k) < 1$, but in general not $\ll 1$), it is clear that the observed linewidths (250–700 Hz) can be accounted for by a very small number of water molecules. The strong orientation dependence of $\Delta\nu$ also suggests a small number of contributing water molecules. These are presumably a subset of the ones contributing to the splitting. Although a contribution from labile BPTI deuterons, especially at 50°C, cannot be ruled out, our linewidths (at pH* 9.5) are similar to those reported for single crystals of lysozyme near pH* 5 (Lauterbur et al., 1978; Borah and Bryant, 1982), where base-catalyzed hydrogen exchange is four orders of magnitude slower than in our crystal. We expect a wide distribution of water residence times at the different sites in a protein crystal. On the basis of the available information on buried water residence times in solution (Denisov et al., 1995, 1996; Halle, 1998), the residence times for some of the buried (W111–113) or intermolecularly trapped waters may well be in the microsecond range.

The longitudinal water $^2$H relaxation rate, $R_1$, has previously been measured (at a single frequency) in polycrystalline samples of crambin, lysozyme, and ribonuclease A (Borah and Bryant, 1982; Usha and Wittebort, 1989; Usha et al., 1991). As in previous studies, we find no deviation from single-exponential relaxation. As noted before (Usha and Wittebort, 1989; Usha et al., 1991), this implies that water exchange between different hydration sites is fast compared to the difference in local relaxation rates (of order 1–10 ms). However, the observation of a homogeneous (exchange averaged) quadrupole doublet imposes a much stronger ($\mu$s) bound on the residence times.

Although previously reported $R_1$ values are on the same order of magnitude as found here (at the corresponding frequency), there are quantitative differences that need to be explained. For monoclinic lysozyme, for example, $R_1 = 33\ s^{-1}$ at 38.7 MHz and 27°C (Usha et al., 1991), increasing to $\sim 80\ s^{-1}$ at 9.2 MHz and room temperature (Borah and Bryant, 1982). For BPTI, we find $R_1$ values of ~100 and 240 $s^{-1}$, respectively, at these frequencies (Fig. 5). The threefold difference in $R_1$ values between lysozyme and BPTI cannot be explained by the different water content of the crystals, because form II BPTI has more water (38 vol%) than monoclinic lysozyme (33 vol%). We believe that the crucial difference is the pH* value, which is 9.5 in BPTI and 4.5 in lysozyme, making base-catalyzed exchange of labile protein deuterons five orders of magnitude faster in our crystal. For the adiabatic linewidth, where the residence time is also the correlation time, fast exchange means that the residence time is shorter than the inverse quadrupole frequency (~1 $\mu$s). Longitudinal relaxation in the MHz range, however, is induced by much faster motions, and fast exchange then only implies a residence time short compared to the local $T_1$ relaxation time (1–10 ms for correlation times of 0.1–10 ns). We conclude, therefore, that labile protein deuterons make a dominant contribution to the $R_1$ data in Fig. 4. Even at the lower pH of the lysozyme crystals, labile deuterons may contribute significantly.

The $R_1$ values obtained from polycrystalline proteins at 38.7 MHz were 15–45 times larger than the relaxation rate in bulk $D_2O$. If this relaxation enhancement is modeled by a single correlation time, one would conclude that water reorientation in the crystal is slowed down by the same factor. From $^{17}$O relaxation dispersion studies of protein solutions, it is known that the water molecules in contact with the protein surface are only slowed down by a factor of 5 on average (Denisov and Halle, 1996). For small solutes such as amino acids, the dynamic retardation factor is about 2 (Ishimura and Uedaira, 1990), suggesting that the larger effect for protein surfaces is dominated by a small number of strongly retarded waters in surface pockets. The finding that the translational self-diffusion coefficient of water in a

single crystal of myoglobin (40 vol% solvent) is only a factor 2 lower than in bulk water (Kotitschke et al., 1990) indicates that most crystal waters have bulk-like dynamics. The larger retardation factors inferred from $R_1$ values would then be due to a minority population of more retarded waters and to local reorientation of rapidly exchanging side-chain deuterons. This is consistent with our $^2$H dispersion (Fig. 5) and a previous $^1$H dispersion from lysozyme crystals (Bryant et al., 1982), showing that $R_1$ remains frequency dependent up to 50 MHz at least. At the frequencies (9.2 and 38.7 MHz) of previous $^2$H $R_1$ measurements, $R_1$, must therefore include a contribution from motions with correlation times in the nanosecond range.

At still lower frequencies, we predict that the $^2$H dispersion exhibits a large step with an apparent correlation time of $\sim$1 $\mu$s, as observed for chemically cross-linked proteins (Koenig et al., 1993; Halle and Denisov, 1995) and colloidal particles (Roose et al., 1999). As predicted theoretically (Halle, 1996), this apparent correlation time is essentially the inverse of the quadrupole frequency and should therefore not depend on temperature. The corresponding $^1$H dispersion should be much broader because of the distribution of intermolecular dipole couplings but should also be insensitive to temperature, features that were indeed observed for lysozyme crystals (Bryant et al., 1982).

## CONCLUSIONS

We have determined the principal components of the motionally averaged quadrupole interaction tensor of the water deuterons in a protein crystal. The analysis of these principal quadrupole frequencies and their temperature dependence, coupled with crystallographically determined water orientations, allowed us to discriminate among models for the orientational order of crystal water. If the protein-water interface were flat, a weakly ordered hydration layer could account for the magnitude of the observed quadrupole splitting. This splitting is attenuated by one to two orders of magnitude, however, because of the nearly isotropic distribution of hydration site orientations on the protein. We therefore attribute the observed splitting (and its temperature dependence) to a small number of highly ordered water molecules, presumably among the internal and intermolecularly trapped crystal waters. The exchange of water molecules in this class, with residence times of order 1 $\mu$s, can also account for the orientation dependence of the $^2$H linewidth. We have also reported the deuteron magnetic relaxation dispersion from the protein crystal and concluded that the observed dispersion in the MHz range is dominated by labile protein deuterons. It therefore cannot be used to make quantitative statements about the rate of water reorientation in the crystal.

Most of the special hydration sites that appear to be responsible for the splitting and linewidth of the $^2$H doublet are located at intermolecular contacts and are thus a property of the crystal rather than the protein. The characteristics of such bridging water molecules are important for crystal stability and protein-protein association in solution, but are irrelevant for protein hydration in dilute aqueous solution. When comparing NMR data on protein surface hydration in solution with diffraction data on crystal waters, it should be kept in mind that some of the most well-defined surface hydration sites in the crystal structure are highly exposed when neighboring protein molecules are removed. As an example, Fig. 10 shows W119 in crystal form II of BPTI. The residence time of a water molecule at this site is likely to be several orders of magnitude longer in the crystal than in solution.

## APPENDIX A: MOTIONAL AVERAGING OF THE WATER $^2$H QUADRUPOLE TENSOR IN AN ORTHORHOMBIC PROTEIN CRYSTAL

In the fast-exchange limit, motional averaging reduces the principal components of the quadrupole interaction tensor according to Eq. 3. By carrying out the transformation from the crystal frame (C) to the molecular principal frame (F) in three steps, via the director frame (D), defined by the local potential of mean torque, and a molecule-fixed frame (M), with the $z$

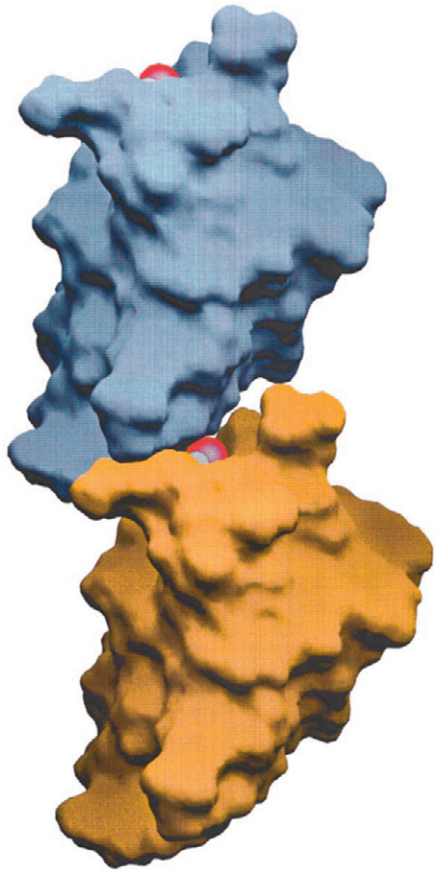

FIGURE 10 A water molecule trapped by protein contacts in crystal form II of BPTI (PDB file 5pti). When a single BPTI molecule is examined, the water molecule W119 appears highly exposed (*top*), but when one of the neighboring 14 BPTI molecules is included, W119 is seen to reside in a deep intermolecular cleft (*center*).

axis along the water $C_{2v}$ axis, the crystal-frame residual anisotropies (in a Cartesian basis) can be expressed as

$$A^{C}_{cc} = \sum_{n} \langle D^{2}_{0n}(\Omega_{CD}) A^{D}_{n} \rangle \tag{A1a}$$

$$A^{C}_{aa} - A^{C}_{bb} = \sqrt{6} \sum_{n} \langle D^{2}_{2n}(\Omega_{CD}) A^{D}_{n} \rangle \tag{A1b}$$

$$A^{C}_{aa} + A^{C}_{bb} + A^{C}_{cc} = 0 \tag{A1c}$$

where $D^{2}_{pn}(\Omega_{CD})$ is an element of the second-rank Wigner rotation matrix and $\Omega_{CD}$ are the Euler angles that effect the transformation between the C and D frames (Brink and Satchler, 1968). The sum runs from $n = -2$ to $n = +2$, and the angular brackets denote an average over all rapidly exchanging water molecules in the asymmetrical unit of the crystal. The director-frame (spherical) residual anisotropies are given by

$$A^{D}_{n} = S_{n0}\sigma_{0} + 2S_{n2}\sigma_{2} \tag{A2}$$

where we have introduced the local order parameters (in a spherical basis)

$$S_{np} = \langle D^{2}_{np}(\Omega_{DM}) \rangle \tag{A3}$$

and the geometric coefficients

$$\sigma_{0} = 1 - \frac{1}{2}(3 - \eta)\sin^{2}\upsilon \tag{A4a}$$

$$\sigma_{2} = -\frac{1}{\sqrt{6}}[1 + \eta - \sigma_{0}] \tag{A4b}$$

where $\eta$ is the asymmetry parameter for the water $^{2}H$ electric field gradient tensor and $2\upsilon$ is the HOH angle. With the standard values, $\eta = 0.11$ and $2\upsilon = 107°$, one obtains $\sigma_{0} = 0.066$ and $\sigma_{2} = -0.426$. Even if a water molecule does not undergo a 180° flip while residing in a hydration site, the two orientations will be exchange averaged. This accounts for the absence of the order parameters $S_{n\pm1}$ and $S_{n-2}$ in Eq. A2. The generalized order parameter that governs relaxation in isotropic solutions is usually defined as (Halle et al., 1999)

$$S^{2} = (1 + \eta^{2}/3)^{-1} \sum_{n} |A^{D}_{n}|^{2} \tag{A5}$$

Unless the 180° flip is fast compared to the isotropic correlation time, $S_{n\pm1}$ will be nonzero, so that $A^{D}_{n}$ in Eq. A5 differs from $A^{D}_{n}$ in Eq. A1.

The general result in Eq. A1 can be simplified in certain special cases. In the limit of rigid binding ($S_{np} = \delta_{np}$), one obtains

$$A^{C}_{cc} = \left(1 - \frac{3}{2}\langle \sin^{2}\theta_{CM} \rangle\right)\sigma_{0} + \frac{\sqrt{6}}{2}\langle \sin^{2}\theta_{CM}\cos(2\phi_{M})\rangle\sigma_{2} \tag{A6a}$$

$$A^{C}_{aa} - A^{C}_{bb} = \frac{3}{2}\langle \sin^{2}\theta_{CM}\cos(2\phi_{C})\rangle\sigma_{0} + \frac{\sqrt{6}}{4}[\langle \cos 2(\phi_{C} + \phi_{M})(1 + \cos\theta_{CM})^{2}\rangle + \langle \cos 2(\phi_{C} - \phi_{M})(1 - \cos\theta_{CM})^{2}\rangle]\sigma_{2} \tag{A6b}$$

If the local order is uncorrelated with the orientation of the hydration site, the two factors in Eq. A1 can be averaged separately. (This includes the limiting case of uniform local order.) If there is also at least threefold symmetry around the local director (so that $A^{D}_{n} = \delta_{n0}A^{D}_{0}$), then Eq. A1 reduces to

$$A^{C}_{cc} = \left(1 - \frac{3}{2}\langle \sin^{2}\theta_{CD} \rangle\right)\langle A^{D}_{0} \rangle \tag{A7a}$$

$$A^{C}_{aa} - A^{C}_{bb} = \frac{3}{2}\langle \sin^{2}\theta_{CD}\cos(2\phi_{C})\rangle \langle A^{D}_{0} \rangle \tag{A7b}$$

## APPENDIX B: LINEWIDTHS IN THE ADIABATIC FAST EXCHANGE REGIME

In the adiabatic regime, where $(\omega_{L}\,\tau_{k})^{2} \gg 1 + (\omega_{Q}\,\tau_{k})^{2}$, the linewidth is governed by the secular term in the spin Hamiltonian. With the Larmor frequency $\omega_{L} \approx 2 \times 10^{8}\ s^{-1}$ and the quadrupole frequency $\omega_{Q} \approx 1 \times 10^{6}\ s^{-1}$, the adiabatic limit is valid for motions with correlation times $\tau_{k} \gg 1/\omega_{L} \approx 5$ ns. Because the linewidth is very large (250–700 Hz), it must be dominated by motions in the microsecond range, for which the adiabatic approximation is valid. In the fast exchange (or motional narrowing) limit, $(\omega_{Q}\,\tau_{k})^{2} \ll 1$, the linewidth $\Delta\nu$ is given by (Abragam, 1961)

$$\Delta\nu = \frac{1}{\pi}\int_{0}^{\infty} d\tau\,[\langle \omega_{Q}(0)\omega_{Q}(\tau)\rangle - \langle \omega_{Q}\rangle^{2}] \tag{B1}$$

where $\omega_{Q}(\tau)$ is the instantaneous quadrupole frequency experienced by a deuteron at time $\tau$. Because the linewidth is dominated by slow motions, we can regard $\omega_{Q}$ as being partially averaged by local water reorientation. From the foregoing analysis of the quadrupole splitting, we know that only a small fraction of the crystal waters are strongly ordered, whereas the majority of waters (contacting exposed parts of the protein surface and forming clusters in interstitial spaces) are only weakly ordered. The correlation time $\tau_{k}$ can then be identified with the water residence time in the $k$th ordered hydration site. Under these conditions, Eq. 5 reduces to

$$\Delta\nu = \frac{1}{\pi N_{uc}} \sum_{k} \langle \omega^{2}_{Qk}\rangle_{uc}\tau_{k} \tag{B2}$$

where the $k$ sum runs over the ordered sites and the average is taken over the full unit cell containing four BPTI molecules and $N_{uc} = 4 \times 160$ water molecules. The quadrupole frequency for a fully ordered water molecule is

$$\omega_{Qk} = \frac{3\pi}{2}\chi \sum_{n}\sum_{p} D^{2}_{0n}(\Omega_{LC}) D^{2}_{np}(\Omega^{k}_{CM})\sigma_{p} \tag{B3}$$

After $\omega_{Qk}$ is inserted, Eq. B2 can be brought to the form of Eq. 2, leading to explicit expressions for the experimentally determined irreducible linewidth coefficients $\Delta\nu_{\lambda}$.

We thank Vladimir Denisov for spectrometer assistance and helpful discussions, Kristofer Modig for preparing Fig. 10, Eva Thulin for performing the dialysis, and Novo Nordisk A/S (Gentofte, Denmark) for a generous supply of BPTI.

This work was supported by the Swedish Natural Science Research Council.

## REFERENCES

Abragam, A. 1961. The Principles of Nuclear Magnetism. Clarendon Press, Oxford.

Baker, E. N. 1995. Solvent interactions with proteins as revealed by x-ray crystallographic studies. *In* Protein-Solvent Interactions. R. G. Gregory, editor. M. Dekker, New York. 143–189.

Blow, D. M., N. E. Chayen, L. F. Lloyd, and E. Saridakis. 1994. Control of nucleation of protein crystals. *Protein Sci.* 3:1638–1643.

Borah, B., and R. G. Bryant. 1982. Deuterium NMR of water in immobilized protein systems. *Biophys. J.* 38:47–52.

Brink, D. M., and G. R. Satchler. 1968. Angular Momentum, 2nd Ed. Clarendon Press, Oxford.

Bryant, R. G., R. D. Brown, and S. H. Koenig. 1982. Nuclear magnetic relaxation dispersion in monoclinic lysozyme crystals. *Biophys. Chem.* 16:133–137.

Denisov, V. P., and B. Halle. 1995. Hydrogen exchange and protein hydration: the deuteron spin relaxation dispersions of bovine pancreatic trypsin inhibitor and ubiquitin. *J. Mol. Biol.* 245:698–709.

Denisov, V. P., and B. Halle. 1996. Protein hydration dynamics in aqueous solution. *Faraday Discuss.* 103:227–244.

Denisov, V. P., B. Halle, J. Peters, and H. D. Hörlein. 1995. Residence times of the buried water molecules in bovine pancreatic trypsin inhibitor and its G36S mutant. *Biochemistry.* 34:9046–9051.

Denisov, V. P., J. Peters, H. D. Hörlein, and B. Halle. 1996. Using buried water molecules to explore the energy landscape of proteins. *Nature Struct. Biol.* 3:505–509.

Denisov, V. P., K. Venu, J. Peters, H. D. Hörlein, and B. Halle. 1997. Orientational disorder and entropy of water in protein cavities. *J. Phys. Chem. B.* 101:9380–9389.

Edmonds, D. T., and A. L. Mackay. 1975. The pure quadrupole resonance of the deuteron in ice. *J. Magn. Reson.* 20:515–519.

Edsall, J. T., and H. A. McKenzie. 1983. Water and proteins. II. The location and dynamics of water in protein systems and its relation to their stability properties. *Adv. Biophys.* 16:53–183.

Fischer, S., C. S. Verma, and R. E. Hubbard. 1998. Rotation of structural water inside a protein: calculation of the rate and vibrational entropy of activation. *J. Phys. Chem. B.* 102:1797–1805.

Frey, M. 1994. Water structure associated with proteins and its role in crystallization. *Acta Crystallogr. D.* 50:663–666.

Gallagher, W., F. Tao, and C. Woodward. 1992. Comparison of hydrogen exchange rates for bovine pancreatic trypsin inhibitor in crystals and in solution. *Biochemistry.* 31:4673–4680.

Gustafsson, S., and B. Halle. 1993. Group theoretical analysis of nuclear spin relaxation in liquid crystals and molecular solids. *Mol. Phys.* 80:549–582.

Halle, B. 1996. Spin dynamics of exchanging quadrupolar nuclei in locally anisotropic systems. *Prog. NMR Spectrosc.* 28:137–159.

Halle, B. 1999. Water in biological systems: the NMR picture. *In* Hydration Processes in Biology. M.-C. Bellisent-Funel, editor. IOS Press, Amsterdam.

Halle, B., and V. P. Denisov. 1995. A new view of water dynamics in immobilized proteins. *Biophys. J.* 69:242–249.

Halle, B., V. P. Denisov, and K. Venu. 1999. Multinuclear relaxation dispersion studies of protein hydration. *In* Biological Magnetic Resonance, Vol. 17. Structure Computation and Dynamics in Protein NMR. N. R. Krishna and L. T. Berliner, editors. Kluwer Academic/Plenum Press, New York. 419–483.

Halle B. and H. Wennerström. 1981. Interpretation of magnetic resonance data from water nuclei in heterogeneous systems. *J. Chem. Phys.* 75: 1928–1943.

Hsi, E., and R. G. Bryant. 1977. Nuclear magnetic resonance relaxation in cross-linked lysozyme crystals: an isotope dilution experiment. *Arch. Biochem. Biophys.* 183:588–591.

Hsi, E., J. E. Jentoft, and R. G. Bryant. 1976. Nuclear magnetic resonance relaxation in lysozyme crystals. *J. Phys. Chem.* 80:412–416.

Ishimura, M., and H. Uedaira. 1990. Natural abundance oxygen-17 magnetic relaxation in aqueous solutions of apolar amino acids and glycine peptides. *Bull. Chem. Soc. Jpn.* 63:1–5.

Islam, S. A., and D. L. Weaver. 1990. Molecular interactions in protein crystals: solvent accessible surface and stability. *Proteins.* 8:1–5.

Iwai, H., A. Sobol, G. Wider, and K. Wüthrich. 1998. The complete surface hydration shell of a protein by NMR spectroscopy. Presented at the XVIIIth International Conference on Magnetic Resonance in Biological Systems, Tokyo, August 1998.

Koenig, S. H., R. D. Brown, and R. Ugolini. 1993. A unified view of relaxation in protein solutions and tissue, including hydration and magnetization transfer. *Magn. Reson. Med.* 29:77–83.

Kotitschke, K., R. Kimmich, E. Rommel, and F. Parak. 1990. NMR study of diffusion in protein hydration shells. *Prog. Colloid Interface Sci.* 83:211–215.

Krüger, G. J., and G. A. Helcké. 1967. Proton relaxation of water adsorbed on protein. *In* Magnetic Resonance and Relaxation. R. Blinc, editor. North-Holland, Amsterdam. 1136–1142.

Lauterbur, P. C., B. V. Kaufman, and M. K. Crawford. 1978. NMR studies of the protein-solvent interface. *In* Cellular Function and Molecular Structure. B. D. Sykes, P. Agris, and R. H. Leppky, editors. Academic Press, New York. 329–351.

Liepinsh, E., G. Otting, and K. Wüthrich. 1992. NMR spectroscopy of hydroxyl protons in aqueous solutions of peptides and proteins. *J. Biomol. NMR.* 2:447–465.

Makinen, M. W., and A. L. Fink. 1977. Reactivity and cryoenzymology of enzymes in the crystalline state. *Annu. Rev. Biophys. Bioeng.* 6:301–343.

Matthews, B. W. 1968. Solvent content of protein crystals. *J. Mol. Biol.* 33:491–497.

Mozzarelli, A., and G. L. Rossi. 1996. Protein function in the crystal. *Annu. Rev. Biophys. Biomol. Struct.* 25:343–365.

Nagendra, H. G., N. Sukumar, and M. Vijayan. 1998. Role of water in plasticity, stability, and action of proteins: the crystal structures of lysozyme at very low levels of hydration. *Proteins.* 32:229–240.

Otting, G. 1997. NMR studies of water bound to biological molecules. *Prog. NMR Spectrosc.* 31:259–285.

Pedersen, T. G., B. W. Sigurskjold, K. V. Andersen, M. Kjœr, F. M. Poulsen, C. M. Dobson, and C. Redfield. 1991. A nuclear magnetic resonance study of the hydrogen-exchange behaviour of lysozyme in crystals and solution. *J. Mol. Biol.* 218:413–426.

Spiess, H. W., and H. Sillescu. 1981. Solid echoes in the slow-motion region. *J. Magn. Reson.* 42:381–389.

Tüchsen, E., and C. Woodward. 1985. Hydrogen kinetics of peptide amide protons at the bovine pancreatic trypsin inhibitor protein-solvent interface. *J. Mol. Biol.* 185:405–419.

Usha, M. G., J. Speyer, and R. J. Wittebort. 1991. Dynamics of the hydrate and amide groups of crystalline ribonuclease and lysozyme. *Chem. Phys.* 158:487–500.

Usha, M. G., and R. J. Wittebort. 1989. Orientational ordering and dynamics of the hydrate and exchangeable hydrogen atoms in crystalline crambin. *J. Mol. Biol.* 208:669–678.

Wagner, G. 1983. Characterization of the distribution of internal motions in the basic pancreatic trypsin inhibitor using a large number of internal NMR probes. *Q. Rev. Biophys.* 16:1–57.

Walter, J., and R. Huber. 1983. Pancreatic trypsin inhibitor. A new crystal form and its analysis. *J. Mol. Biol.* 167:911–917.

Wittebort, R. J., E. T. Olejniczak, and R. G. Griffin. 1987. Analysis of deuterium nuclear magnetic resonance line shapes in anisotropic media. *J. Chem. Phys.* 86:5411–5420.

Wlodawer, A., J. Walter, R. Huber, and L. Sjölin. 1984. Structure of bovine pancreatic trypsin inhibitor. Results of joint neutron and x-ray refinement of crystal form II. *J. Mol. Biol.* 180:301–329.